Atmos. Chem. Phys. Discuss., 6, 8383–8419, 2006
www.atmos-chem-phys-discuss.net/6/8383/2006/

Atmospheric Chemistry and Physics Discussions

Reevaluation of mineral aerosol radiative forcings suggests a better agreement with satellite and AERONET data

Y. Balkanski[1], **M. Schulz**[1], **T. Claquin**[1,*], **and S. Guibert**[1]

[1]Laboratoire des Sciences du Climat et de l'Environnement, 91190 Gif-sur-Yvette Cedex, France
[*]now at: CDC IXIS CAPITAL MARKETS, Paris, France

Received: 27 March 2006 – Accepted: 22 June 2006 – Published: 1 September 2006

Correspondence to: Y. Balkanski (yves.balkanski@cea.fr)

Abstract

Modelling studies and satellite retrievals do not agree on the amplitude and/or sign of the direct radiative perturbation from dust. Modelling studies have systematically overpredicted mineral dust absorption compared to estimates based upon satellite retrievals. In this paper we first point out the source of this discrepancy, which originates from the shortwave refractive index of dust used in models. The imaginary part of the refractive index retrieved from AERONET over the range 300 to 700 nm is 3 to 6 times smaller than that used previously to model dust. We attempt to constrain these refractive indices using a mineralogical database and varying the abundances of iron oxides (the main absorber in the visible). We first consider the optically active mineral constituents of dust and compute the refractive indices from internal and external mixtures of minerals with relative amounts encountered in parent soils. We then compute the radiative perturbation due to mineral aerosols for internally and externally mixed minerals for 3 different hematite contents, 0.9%, 1.5% and 2.7% by volume. These amounts represent low, central and high content of iron oxides in dust determined from the mineralogical database. Based upon values of the refractive index retrieved from AERONET, we show that the best agreement between 440 and 1020 nm occurs for mineral dust internally mixed with 1.5% volume weighted hematite. This representation of mineral dust allows us to compute, using a general circulation model, a new global estimate of mineral dust perturbation between –0.40 and –0.21 Wm^{-2}. This range is determined from both optical properties and varying dust size distribution. The broadband shortwave effect varies from –0.78 to –0.53 Wm^{-2} and the longwave effect between +0.29 and +0.38 Wm^{-2}. The 24-h average atmospheric heating by mineral dust during summer over the tropical Atlantic region (15° N–25° N; 45° W–15° W) is in the range +22 to +32 Wm^{-2} τ^{-1} which compares well with the 30±4 Wm^{-2} τ^{-1}measured by Li et al. (2004) over that same region. The refractive indices from Patterson et al. (1977) and from Volz (1973) overestimate by a factor of 2 the energy absorbed in the column during summer over the same region.

ACPD
6, 8383–8419, 2006

1 Introduction

The direct radiative effect (DRE) of mineral aerosols or perturbation has important bearings on the state of the atmosphere. For non-absorbing aerosols, scattering restricts the solar radiation reaching the surface and leads to the cooling of the atmospheric column. For an absorbing aerosol, the fraction of the solar radiation trapped in the aerosol layer added to the absorption of the terrestrial radiation warms the atmospheric column. What distinguishes mineral aerosol from other aerosol components is that it will either cool or warm the atmospheric column depending on the land surface albedo. The refractive index is the source of a great part of the uncertainty in estimating dust DRE, other sources of uncertainty include, by order of importance, the particle size distribution, the vertical distribution, cloud albedo and the albedo of the underlying surface (Liao and Seinfeld, 1998).

Previous published estimates of dust DRE have relied upon the values of refractive indices published by Patterson et al. (1977), Volz (1973), D'Almeida et al. (1991), Shettle and Fenn (1979) and Sokolik et al. (1993), Fig. 1a. Based on these reported imaginary part of the refractive index, Fig. 2 of Claquin et al. (1998), attempted to define minimum and maximum values over both shortwave and longwave spectra. The reported values over the spectral range 0.3 to 30 μm span from a factor of five to an order of magnitude. Such large uncertainties in the refractive index do not put a constraint on whether dust absorption leads to a cooling or a warming of the atmospheric column over most surfaces.

As of today, coupled climate models and forecast models do not include the radiative effect of mineral aerosols in great part due to these uncertainties. Dust has been shown to affect weather forecast in tropical regions (Alpert et al., 1998). Hence, it is important to address the uncertainty in the radiative effect of mineral dust. This paper uses data that recently became available from the AERONET sunphotometer network, to re-evaluate the validity of earlier refractive indices and present some possible reasons for discrepancies between the refractive indices published.

ACPD
6, 8383–8419, 2006

The first investigation that drew into question the absorption of dust in modelling papers is the work of Kaufman et al. (2001). These authors examined the contrast of two dusty situations off the coast of Africa when optical depth reached 0.8 and 2.4 at 640 nm. The imaginary part of the dust refractive index was varied for these two cases until it fitted the radiances computed from the surface reflectance at satellite level. The increase in apparent reflectance that is consistent for the whole area of study suggested that dust is close to non-absorbing. Independently, Moulin et al. (2001) noticed that the spectral reflectance measured from the Sea-viewing Wide Field-of-view Sensor (SeaWiFS) in dusty conditions could be matched only by decreasing the imaginary part of mineral aerosol refractive index (see Table 4 of Moulin et al., 2001). These findings were confirmed through the study of Haywood et al. (2003) who analysed important episodes of dust transported between Dakar (14.7° N, 17.3° W) and Sal Island (16° N, 24° W).

The first part of this paper compares AERONET retrieved refractive indices (Dubovik et al., 2002) to other published refractive indices. The second part presents how the distribution of dust used in these computations was obtained from a General Circulation Model (GCM) coupled to a chemical/aerosol module. The third part follows a recommendation made in the conclusions of the 1st International workshop on Mineral Aerosols (Sokolik, 1999): we include the mineralogical composition of dust in a more realistic way in the model through the treatment of the principal components in terms of optical properties. We then compute the annual mean dust radiative forcing at the top of the atmosphere and at the surface in part 4 by varying mineralogical composition for different assumptions of internally mixed and externally mixed minerals. In part 5, the column heating is compared with previous reports of clear sky shortwave radiative forcing by mineral dust off-coast western Africa. Finally we discuss in part 6 whether mineral dust is warming or cooling the atmospheric column.

ACPD
6, 8383–8419, 2006

2 Dust refractive indices

Works from Liao and Seinfeld (1998), Sokolik and Toon (1999) and from Claquin et al. (1999) have discussed the main sensitivities of the dust radiative perturbation to its mineralogical content and to the representation of the size distribution. Sokolik and Toon (1999) and Claquin et al. (1999) showed that dust mineralogy can be represented with six main minerals: illite, montmorillonite, kaolinite, quartz, calcite and hematite.

For each mineral the real and imaginary part have been defined spectrally and we indicate the refractive indices that are used in this study in Table 1 (see also Table 3 Sokolik and Toon, 1999). We use the mineralogical database described by Claquin et al. (1999) to derive the absorption of mineral dust with hematite contents characteristic of arid and semi-arid regions.

Absorption by mineral dust in the shortwave is mostly due to the presence of iron oxides in the form of hematite. The mineralogical database over arid and semi-arid areas allows to search for the fraction of hematite in mineral dust relative to the other minerals present. 1%, 5%, 50%, 95% and 99% of the areas of the database have a volume weighted hematite of more than 3.4, 2.7, 1.5, 0.9 and 0.8%, respectively. In this paper, we will refer to the 1.5% hematite content as our reference case and note it as *S1*, the hematite content of 2.7 and respectively 0.8% will be referred to as *S1b* and *S1c* in simulations conducted with the LMDz-INCA model described below. Since most of the variations in absorption in the shortwave are caused by hematite, we kept constant the relative volume of the other minerals for these 3 cases and only adjusted the illite content (see Table 2). In order to check that other mineralogical variations do not affect the results presented we also varied the other minerals in sensitivity cases.

To contrast the refractive indices of these 3 cases to the refractive indices proposed by Patterson et al. (1977) and by Volz (1973), we refer to the simulation with a single set of refractive indices from Patterson and Volz as *S2*. In simulation *S2*, we constructed the refractive indices in the range 700 to 2500 nm by interpolating linearly between the values of Patterson et al. (1977) and Volz (1973).

ACPD
6, 8383–8419, 2006

2.1 Dielectric model, refractive index for internally mixed minerals

Atmospheric dust sample show that hematite is generally embedded in a matrix made of the other mineral constituents. Therefore, an optical model is needed to derive the refractive index of these minerals as an internal mixture.

For a homogeneous matrix in which spheres are present, the Maxwell-Garnet approximation allows to compute a resulting refractive index for the mineral aggregate. Following this approximation, the complex refractive index, n_{agg}, can be written as a function of the refractive indices of the matrix, n_m, and of the inclusion, n:

$$n_{agg} = n_m \left\{ \left(1 + \left[\frac{3v\,(n - n_m)}{n + 2n_m}\right]\right) \left(1 - \frac{v\,(n - n_m)}{n + 2n_m}\right)^{-1} \right\} \quad (1)$$

The refractive index of the mixed aerosol, $n_{mixture}$ is then obtained from n_{agg} as:

$$n_{mixture} = (n_{agg})^{1/2} \quad (2)$$

where n_m is the complex refractive index of the matrix, v is the ratio of the volume of the inclusion to the total volume, and n is the complex refractive index of the inclusion.

Since refractive indices and radiative forcing by aerosols have been reported either for the shortwave only or for both shortwave and longwave, we treat them separately in order to be able to compare the results of this study to previously published ones.

A straightforward comparison of dust refractive indices reported by Patterson et al. (1977) and by Volz (1973) to AERONET measurements (Fig. 1) indicates that models have overestimated mineral dust absorption. Over the spectral region documented by Patterson and al. (1977) (i.e. between 300 and 700 nm) the imaginary part of the refractive index is one order of magnitude greater than the value retrieved from AERONET measurements. When we take the upper end of the uncertainty range in the AERONET measurements, Patterson et al. (1977) values are still a factor 5 to 9 larger over this same spectral range. The consistency of the values of refractive indices retrieved from AERONET over all sites where mineral dust is the dominant aerosol

ACPD
6, 8383–8419, 2006

component suggests that the absorption of airborne mineral dust is lower than the values of Patterson et al. (1977) and by Volz (1973). We also compared these values with two other sets of mineral dust refractive indices that have been used in modelling work. The first one is the refractive indices reported by d'Almeida et al. (1991) that are part of the Global Aerosol Climatology where the spectral range for mineral aerosol refractive index spans from 300 to 4000 nm. These measurements show similar discrepancies at the two wavelengths 440 and 670 nm, whereas the comparison with the AERONET shows a much better agreement at 870 and 1020 nm (Top panel, Fig. 2). In a different set of measurements of Shettle and Fenn (1979), the imaginary part of the refractive index is overestimated by a factor 4 to 10 for the 4 wavelengths reported when compared with AERONET measurements (Bottom panel, Fig. 2).

Figures 3 and 4 show the refractive indices of dust for 2 hypotheses of mixing: one for a volume weighed average aggregate of minerals (Fig. 3) and the second one for hematite imbedded in a matrix made of quartz, calcite, illite, kaolinite or montmorillonite (Fig. 4). When minerals are treated as a volume weighted average, the imaginary part of the refractive index is within or close to the range of uncertainty indicated in AERONET measurements at the 4 wavelengths. In contrast, for the high hematite content (2.7% by volume), this imaginary part is just as large as in the case of the Patterson et al. (1977) measurements or of d'Almeida et al. (1991) at wavelengths 440 and 670 nm.

When minerals are considered as an internal mixture of minerals with embedded hematite, at all 4 AERONET wavelengths (440, 670, 870 and 1020 nm) the mixture with low hematite content (0.9%) and the mixture with high hematite content (2.7%) bracket the imaginary values reported by Dubovik et al. (2002). Not only does the imaginary part of the refractive index agree well with the ranges measured in AERONET but the constraint set by the real part is also satisfied. The central value of 1.5% hematite is in very good agreement with these measurements (see Fig. 4). For the longwave, the refractive indices were compared with Sokolik et al. (1999). We checked that no large difference in refractive indices was found over the spectral interval: 3 to 30 μm. The

ACPD
6, 8383–8419, 2006

discussion in this paper is primarily focused on the shortwave spectrum.

The mineralogically based approach that was first proposed by Sokolik et al. (1999) helps us reconcile the derived refractive indices with the measured ones.

3 Model and methods

3.1 LMDZ-INCA

LMDz-INCA stands for a coupled General Circulation Model (LMDz) described by Hourdin et al. (2006) with a Chemistry-Aerosol module (INCA). The INCA (Interactions between Chemistry and Aerosols) module includes the treatment of gases important in the radiative budget (CO_2, CH_4, CO, CFCs, and HCFCs, see Hauglustaine et al., 2004) as well as of the different aerosol components (sulphate, BC, organic, dust, and seasalts). In order to be computationally efficient and accurate, a modal scheme for particle size distribution has been adapted to treat an aerosol population. This allows to follow the size distribution of the aerosol with only two tracers per mode (one tracer follows the mass, and a second one follows the number distribution). Hence, it reduces the number of tracers by as much as an order of magnitude with a comparable precision in the computation (see Schulz et al., 1998). The drawback of the modal scheme is that the number of modes is set at the beginning of the run and it is difficult to add modes to the distribution. In addition, an implicit assumption is made that the processes such as deposition and chemical transformation do not affect the width of the size distribution but only its mass median diameter. The merits of this approach have been discussed for: an episode of dust transport across the Mediterranean Sea in Schulz et al. (1998), a comparison of dust optical depth to satellite data in Guelle et al. (2000), and an extensive comparison of sea-salts to measurements of size distribution in the coarse and fine modes in Guelle et al. (2001).

The wet scavenging scheme distinguishes between stratiform and convective precipitation. Both types of precipitation are treated separately and parameterised as a

ACPD
6, 8383–8419, 2006

EGU

first-order loss process (Giorgi and Chameides, 1985).

$$dC_g/dt = -\beta C_g \quad (3)$$

where C_g is the aerosol concentration in the gas phase and β the scavenging coefficient (s^{-1}). The rain liquid water content (L) is derived from the total (solid + liquid) water flux calculated by the GCM. Rainout by snow occurs with the same efficiency as liquid water. The scavenging by convective precipitation is calculated as part of the upward convective mass flux based on a modified version of the scheme proposed by Balkanski et al. (1993). Based on this formulation and on the previous equation, we derive for the scavenging coefficient associated with convective precipitation:

$$\beta^{cv} = -fF_u g/p \quad (4)$$

where f is the fraction of aerosol removed, F_u, the upward convective mass flux diagnosed by the GCM (kg m^{-2} s^{-1}), and g, the gravity constant. We assume as in Liu et al. (2001) that for convective events, the fraction, f, of aerosol removed is:

$$f = (1 - e^{-\alpha \Delta z}) \quad (5)$$

where Δz [m] is the height in the convective tower calculated from the cloud base. The scavenging efficiency α [m^{-1}] is ratio of the rate constant for conversion of cloud water to precipitation (C_{pr}) and the updraft velocity w. Based on Mari et al. (2000) and Liu et al. (2001), we adopt C_{pr}=5×10^{-3} m s^{-1}, w=10 m s^{-1} leading α=5×10^{-4} m^{-1}.

3.2 Treatment of the dust emissions

Dust emissions in the model follow Schulz et al. (1998) and Guelle et al. (2000). The dust fluxes are calculated as a function of soil threshold velocities and wind friction velocities, which are in turn parameterized as a function of the soil particle size and the surface roughness length. Then the dust emission fluxes are determined according to the clay content of eroding soil. This formulation has been shown to give very

good agreement with measurements of dust mass concentrations and AODs in previous global modeling studies (Schulz et al., 1998; Guelle et al., 2000). To account for the high spatial variability in horizontal wind speeds, dust emission fluxes have been generated off line using ECMWF 6-hourly horizontal 10-m wind speeds at a resolution of $1.125^\circ \times 1.125^\circ$ and are regridded to the model resolution of $3.75^\circ \times 2.5^\circ$. Dust emission is inhibited in the model when humidity persists over the upper soil layer following precipitation. Soil humidity is estimated through a simple bucket equation. We use a spectral description of the size distribution with a mass median diameter (MMD) of 2.5 μm (modal diameter of 0.59 μm) at the source and a width σ=2.0 (see Schulz et al., 1998). We will see that a coarse mode with an MMD of 5.0 μm (modal diameter of 1.18 μm) changes the optical depth in the source regions but has little effect over distant areas.

We present in Figs. 5 and 6 the comparison of AERONET retrieved optical depths to the simulated ones at 5 sites, 3 over Africa and the tropical Atlantic (Dakar, Cape Verde and Barbados) and 2 sites over the Arabian Peninsula (Bahrain and Solar Village). These sites were chosen for their position along the main pathway of dust transport and were used by Dubovik et al. (2002) to retrieve the refractive indices of dust for 3 of them (Cape Verde, Bahrain and Solar Village). The seasonality is well reproduced and the amplitude of the optical depth agrees well with these observations.

3.3 Radiative code

The radiative code in the LMDZ GCM consists of an improved version of the parameterizations of Fouquart and Bonnel (1980) (solar radiation) and Morcrette (1991) (terrestrial radiation). The shortwave spectrum is divided into two intervals: 0.25–0.68 and 0.68–4.00 μm, respectively, and the longwave spectrum is divided into 5 intervals. The model accounts for the diurnal cycle of solar radiation and allows fractional cloudiness to form in a grid box. In the cloud-free portion of the grid box, the optical properties of aerosols are combined and a delta approximation of the forward scattering peak is made to account for the highly asymmetric aerosol phase function. The reflectiv-

ity and transmissivity of a layer are computed using the random overlap assumption (Morcrette and Fouquart, 1986) by averaging the clear and cloudy sky fluxes weighted linearly by their respective fractions in the layer. The radiative fluxes are computed every two hours, at the top-of-atmosphere and at the surface, with and without the presence of clouds, and with and without the presence of aerosols. The clear-sky and all-sky aerosol radiative forcings can then be estimated as the differences in radiative fluxes with and without aerosols.

4 Modelled direct radiative forcing of mineral dust

4.1 Influence of the different sets of refractive indices

We present in Fig. 7 the top of atmosphere (TOA) aerosol radiative forcing of dust for two cases of refractive indices: The simulation referred as *S2* where refractive indices used are the ones reported by Patterson et al. (1977) and Volz (1973) and the simulation *S1* for which the 5 most abundant minerals are internally mixed with 1.5% hematite. The refractive indices from *S1* characterized in Sect. 2, showed a very good agreement with the AERONET retrieved indices at the 4 wavelengths. For these two cases, the effect of mineral dust absorption is dramatically different over both continents and oceans (Fig. 7). Over continents, the sign of the forcing depends mainly on the albedo of the surface and can also be influenced by the presence of clouds below the aerosol layer. When the yearly averaged surface albedo reaches values greater than 0.2, the shortwave radiative forcing turns positive. The presence of low level clouds over surface albedos between 0 and 0.2 will lead to a positive TOA forcing if clouds are present below the aerosol layer throughout the year. Table 3 summarizes the resulting forcing which averages the positive and negative contributions over oceanic and continental regions. Over arid and semi-arid areas such as the Sahara and the Arabian Peninsula, dust radiative forcing is much more positive in the hypothesis of the *S2* simulation compared with *S1*. The more dramatic differences occur for 3 continental

ACPD
6, 8383–8419, 2006

regions the Sahel, the Arabian Peninsula and Asia where the sign of the TOA forcing is negative for the simulation *S1* and positive for *S2*. Over the tropical Atlantic, and North Indian Ocean both TOA and surface radiative forcing from dust have negative signs in *S1* and *S2* cases. The atmospheric heating is 3 to 4 times smaller in the *S1* than in the *S2* simulation over these regions. Over the Sahara region, the TOA forcing from mineral dust changes is positive for both cases. The heating over the Saharan region is also 4 times smaller in *S1* compared to the *S2* case (Table 3).

4.2 Shortwave versus Longwave TOA radiative forcing

Figure 8 presents respectively the shortwave (top panel) and longwave (middle panel) contribution to the TOA forcing for the *S1* case. Globally averaged, the shortwave and longwave TOA forcings amount respectively to –0.68 and +0.29 Wm^{-2}, the overall forcing is –0.39 Wm^{-2}. Top of the atmosphere shortwave forcing is always negative over dark surfaces such as the oceans in agreement with findings of Liao and Seinfeld (2001, Figs. 1 and 2) when clouds are not permanently present. The bottom panel of Fig. 8 presents the yearly average TOA forcing from dust (SW+LW). Over bare surfaces the forcing is positive and can reach +2 to +5 Wm^{-2} over source regions in Sahara or over the Arabian Peninsula. In contrast, regions with the strongest negative forcing are the Eastern tropical Atlantic and the Northern Indian Ocean, large regions over which the yearly mean minimum forcing is between –5 to –20 W m^{-2}.

In order to evaluate the DRE when the refractive indices of Patterson-Volz are used, we ran the model with the same size distribution clouds and scavenging scheme and computed the direct radiative effect for case *S2* (see Table 4). The TOA forcing computed turns also positive with a value of +0.35 Wm^{-2} globally and which consists of an overall positive SW TOA (+0.05 Wm^{-2}) forcing combined with a LW TOA forcing of +0.30 Wm^{-2} as summarized in Table 4.

We now compare these values from Tegen et al. (1996), Woodward (2001) and Myrhe and Stordal (2001) with the *S2* simulation (Table 4). In all these studies the refractive indices used over the spectral intervals 300–700 nm and 2500–4000 nm have

values close to the *S2* simulation. Woodward (2001) tried to create representative values, by taking the average of the extremes of a range of measurements at each wavelength from the compilation of measurements from Carlson and Benjamin (1980), Sokolik et al. (1993, 1998), WMO (1993). This leads to an imaginary part of the refractive index which is 3 to 5 times greater than for the AERONET values as the wavelength increases from 440 to 1020 nm. The TOA radiative effect from dust aerosols in the shortwave was reported to be: –0.39 Wm^{-2} in Tegen et al. (1996), –0.61 Wm^{-2} with the same aerosol distribution by Myrhe and Stordal (2001), –0.16 in the work of Woodward (2001). We can only point out to the different possibilities that could account for these differences: differences in the refractive indices in the remaining window from 700 to 2500 nm, different heights for the mineral dust distribution and differences in the radiative code or in water clouds. Clearly, it would be worthwhile focusing on the source of these differences but this is beyond the scope of this paper.

4.3 Variation of the forcing with the hematite content in dust

We also studied the influence of the amount of hematite on the radiative forcing for the 3 hematite contents representative of low, central and high abundances of iron oxides in dust. The main differences in the radiative forcing at the top of the atmosphere can be seen over land for the two extremes cases *S1b* and *S1c* of low and high hematite (Fig. 9). The main areas where the hematite content changes the magnitude of the TOA forcing are over the 2 of the main source regions, the Sahara and the Arabian Peninsula. For the *S1b* case (Fig. 9), this forcing remains in the range between 0 and +2 Wm^{-2}. It approximately doubles over these regions when the hematite content corresponds to the more absorbing aerosol *S1c* and averages between +2 and +5 Wm^{-2}. The global annually averaged radiative forcing at the top of the atmosphere is presented for the 3 cases in Table 5 and the values lie between –0.47 and –0.24 Wm^{-2}. The surface radiative forcing varies over a narrower range between –1.11 and –0.81 Wm^{-2}. These results show the sensitivity of the dust radiative forcing to the hematite content.

ACPD
6, 8383–8419, 2006

4.4 External mixing

The process of saltation which is the bombardment of mineral aerosol aggregates at the surface is the prelude to their injection in the atmospheric boundary layer. Following saltation, the minerals transported in the atmosphere can be either in the form of external or internal mixtures. In the case of an external mixture, the different minerals can be treated independently and assuming that the size distribution has been characterized, then with the assumption that the non-sphericity of dust has little influence on the radiative perturbation (Mischenko et al., 1997) one can infer from Mie theory the optical parameters necessary for estimating the radiative effect of dust. Although we have shown by comparison with the AERONET retrieved refractive indices that the internally mixed case for minerals better represents the observed mineral dust optical properties, it is instructive to discuss the forcings as we treat dust as internally versus externally mixed minerals. The main differences in the TOA forcing occur for an external mixture of minerals with high hematite content (see Table 5, case *S3c*). Over most of the continental regions where dust is abundant; the TOA forcing exceeds 1 Wm^{-2} and reaches 10 Wm^{-2} over Western Sahara (not shown). These large positive forcings over continental areas with high dust loads lead to a global mean TOA forcing of +0.17 Wm^{-2} (Table 5). We rule out the possibility of an external mixture with high hematite based upon the refractive index computed for such an assembly of minerals. Such a case would imply an imaginary part of the refractive index that exceeds AERONET retrievals by as much as an order of magnitude for certain wavelengths. In the case of an internal mixture with a hematite core, the top-of-atmosphere forcing rarely exceeds 5 Wm^{-2} over Sahara and the TOA global average is –0.24 Wm^{-2}.

In the case of the lower hematite contents (respectively 0.5 and 1.0%) reported by Myrhe and Stordal (2001) in Table 5, the net flux at the top of the atmosphere is smaller than for case *S1* as one would expect since these aerosols are less absorbing.

ACPD
6, 8383–8419, 2006

4.5 Sensitivity of the forcing to the dust size distribution

To investigate the sensitivity of this forcing to the variation in size distribution, we vary in case *S4* the size spectrum of the dust in our 3-D INCA model. We added to the standard case with one mode (MMD=2.5 μm equivalent to a modal diameter of 0.59 μm with a width σ=2.0), a coarse mode with an MMD of 5.0 μm (modal diameter of 1.18 μm and σ=2.0) at the point of injection. The optical depth of the coarse mode alone vanishes due to sedimentation as soon as dust is transported beyond the West Coast of Africa. Hence, the coarse mode alone with the narrow distribution we are studying here cannot by itself explain the optical depths seen by sensors such as MODIS across the tropical Atlantic Ocean whereas both the coarse and the fine mode will. The resulting forcing at the top of the atmosphere reaches then –0.40 Wm^{-2} (Table 4), a value very close to the standard simulation with a smaller aerosol mode as the decrease in the shortwave forcing is compensated by a significant increased in the longwave. With this additional coarse mode, the radiative forcing at the surface decreases by 23% (from –0.92 to –1.13 Wm^{-2}).

5 Comparison of mineral dust clear-sky forcing efficiency with measurements in the tropical Atlantic

The broadband shortwave direct radiative effect from dust has been inferred using the synergy of different satellite and assumptions on the refractive indices and the size distribution of the dust aerosols. Li et al. (2004) using the synergy of the data from CERES (Clouds and Earth Radiant Energy System) and from MODIS (Moderate Resolution Imaging Spectroradiometer) were able to determine the aerosol clear-sky forcing efficiency for two seasons: summer and winter. These measurements took place over the tropical Atlantic region (45° W–15° W and 15° N–25° N). During summer (JJA) when dust loads are high, the TOA clear-sky forcing efficiency is estimated to be –35 Wm^{-2} τ^{-1}, and –65 Wm^{-2} τ^{-1} at the surface. In contrast, during winter, the

clear-sky TOA forcing efficiency, when dust loads are relatively low and carbonaceous aerosols are present, is –26 Wm^{-2} τ^{-1}, and –81 Wm^{-2} τ^{-1} at the surface. We present in Table 6 the comparison with the clear-sky forcing efficiency obtained in this study.

Since we wanted to be in conditions where the only aerosol was dust, we limit the comparison to the summer season when the single scattering albedo is 0.95 (Li et al., 2004), indicative that dust is by far the dominant aerosol component. The much lower winter single scattering albedo of 0.86 obtained during the dry season indicates the presence of carbonaceous aerosols produced by biomass burning. The TOA direct radiative efficiency for clear-sky conditions varies from –45 to –49 Wm^{-2} τ^{-1} for the 3 hematite contents discussed here. These values are lower than the -35 ± 3 Wm^{-2} τ^{-1} measured by Li et al. (2004). In contrast the refractive indices of Patterson et al. (1977) and Volz (1973) lead to a TOA direct radiative efficiency of –29 Wm^{-2} τ^{-1}.

Li et al. (2004) measurements report a value of $+30\pm4$ Wm^{-2} τ^{-1} (–35–(–65)) for the column heating efficiency. The amount of energy absorbed in the atmospheric column is best represented by the case 2.7% hematite when this efficiency is +32 Wm^{-2} τ^{-1}. The Patterson-Volz case (*S2*) overestimates by a factor of 2 the absorbing efficiency of mineral dust.

The ratio of surface to top of atmosphere forcing efficiency also indicates if dust radiative properties are captured. A summer ratio of 1.9 can be computed from Li et al. (2004) measurements. The summer ratio is in the range 1.5 to 1.7 for cases *S1* and *S1c* close to the measurements, whereas the value of 1.3 for the lower hematite content indicates too little absorption for the case *S1b*. In contrast, case *S2* when refractive indices from Patterson et al. (1977) and Volz (1973) are used leads to a ratio of 3.0 largely overestimating the observed one (Table 6).

The SHADE experiment took place in September 2000 near Dakar (14° N, 17° W). Haywood et al. (2003) and Anderson et al. (2005) inferred the DRE from airborne measurements of the radiation. A very intense dust episode was observed on 30 September when optical depth reached 1.49 at 550 nm at 12:30 UTC. In Anderson et al. (2005) the authors computed the diurnal average radiative forcing efficiency to be

–24 Wm^{-2} τ^{-1} and found that the ratio between instantaneous and diurnal mean was 3.6. In addition, Haywood et al. (2003) were able to estimate the ratio of surface to top of atmosphere radiative forcing efficiency at 1.6 which allowed us to compute the surface value given in Table 6. The simulated DRE for cases *S1*, *S1b* and *S1c* lead to values from –16 to –24 Wm^{-2} τ^{-1} very close to the diurnal mean observed. The efficiency at the surface are overestimated, from –48 to –57 Wm^{-2} τ^{-1} as compared to the inferred value by Haywood et al. (2003) of –38 Wm^{-2} τ^{-1}. In contrast case *S2*, Patterson-Volz, leads to a simulated positive forcing efficiency of +4 Wm^{-2} τ^{-1} and a very large value at the surface of –70 Wm^{-2} τ^{-1} close to 2 times the inferred value. Once again we conclude that such aerosol is much more absorbing than the measurements indicate.

6 Discussion: Is dust warming or cooling the atmospheric column?

Mineral aerosols have a much contrasted radiative effect depending upon the brightness of the underlying surface. Over bare surfaces with a large surface albedo (>0.30) the mineral aerosols will always warm the atmospheric column. Over dark surfaces such as oceans and deciduous forests, where surface albedo is less than 0.15, the effect of the mineral aerosols is similar to sulphates since it cools the atmospheric column. Over surface albedos in the intermediate range, $0.15<A<0.30$, the sign of the forcing depends mainly on two factors, the size distribution and the mineralogical composition, both of which determine the single scattering albedo of the particles.

The refractive indices computed in this study are coherent with the measurements. In addition, these refractive indices lead to radiative forcing efficiency close to what was observed over the Western tropical Atlantic. The 3 experiments for which the agreement was obtained were respectively internal mixtures with 1.5 and 2.7% hematite and the sensitivity case with 1.5% hematite when a coarse mode is added to the initial size distribution. From these 3 cases, we bracket the global top-of-atmosphere radiative forcing of dust in between values of –0.40 Wm^{-2} and –0.24 Wm^{-2}. For the surface

forcing, the range of these 3 cases is within –1.11 Wm^{-2} and –0.92 Wm^{-2}. In terms of energy stored in the column per unit optical depth of mineral dust, the energy stored is +31 Wm^{-2} τ^{-1} for the Saharan region and 33 Wm^{-2} τ^{-1} or the Arabian Peninsula.

7 Conclusions

In this paper we examined of mineral aerosol refractive indices. A database of soil mineralogy from arid and semi-arid regions determined the mineralogical composition. The radiative properties of an internal mixture of minerals containing 0.9, 1.5 and 2.7% hematite were presented that respectively represent: low, median and high absorption.

The top of atmosphere and surface radiative forcing were determined under these assumptions. We found a top of atmosphere radiative forcing in the range from –0.47 to –0.24 W m^{-2} and a surface radiative forcing from –0.81 to –1.13 W m^{-2}. These values indicate that dust is less absorbing than previously assumed (the top of the atmosphere radiative forcing reaches +0.35 Wm^{-2} and the surface forcing, –1.44 Wm^{-2}, with the same assumptions of dust spatial distributions and clouds when we use refractive indices from Patterson et al., 1977, and Volz, 1973).

We compared our results with summer measurements of direct radiative forcing efficiency over the Atlantic region (45° W–15° W and from 15° N to 25° N) to measurements taken during the SHADE experiment near Dakar in September 2000. Both cases with median and high hematite contents (*S1 and S1c*) lead to radiative forcing efficiencies that are consistent with the measurements of Li et al. (2004). In contrast, the case *S2* with refractive indices from Patterson et al. (1979) and Volz (1977) overestimates the heating by a factor of 2 and the ratio of surface to top of atmosphere radiative forcing efficiency by a factor of 3.

The disagreements in dust absorption between satellite retrieved effects (Kaufman et al., 2000, Moulin et al., 2000, and Haywood et al., 2003), and the modelling studies have been solved through the evaluation of dust refractive indices from the primary minerals that constitute this aerosol. We argue, as these authors did using satellite

measurements, that dust is less absorbing than previously thought.

Acknowledgements. This paper is dedicated to Y. Kaufman. The authors would like to acknowledge discussions with O. Dubovik, C. Textor, F. Dentener, O. Boucher, S. Woodward and J. Haywood. We are grateful to the AERONET network for making their measurements available. This work was funded by the European projects Phoenics EVK2-CT-2001-00098 and as part of GEMS FP6-2003-SPACE 1.

References

Alpert, P., Kaufman, Y. J., Shay-el, Y., Tanré, D., da Silva, A., Schubert, S., and Joseph, Y. H.: Dust forcing of climate inferred from correlations between dust data and model errors, Nature, 395, 367–370, 1998.

Anderson, T. L., Charlson, R. J., Bellouin, N., Boucher, O., Chin, M., Christopher, S. A., Haywood, J., Kaufman, Y. J., Kinne, S., Ogren, J. A., Remer, L. A., Takemura, T., Tanré, D., Torres, O., Trepte, C. R., Wielicki, B. A., Winker, D. M., and Yu, A. H.: An "A-Train" Strategy for Quantifying Direct Climate Forcing by Anthropogenic Aerosols, BAMS, 86(12), 1795–1809, doi:10.1175/BAMS-86-12-1795, 2005.

Balkanski, Y., Jacob, D. J., Gardner, G. M., Graustein, W. C., and Turekian, K. K.: Transport and residence times of tropospheric aerosols inferred from a global three-dimensional simulation of 210Pb, J. Geophys. Res., 98, 20 573–20 586, 1993.

Bedidi, A. and Cervelle, B.: Light scattering by spherical particles with hematite- and goethite-like optical properties.Effect of water impregnation, J. Geophys. Res., 98, 11 941–11 952, 1993.

d'Almeida, G. A., Koepke, P., and Shettle, E. P.: Atmospheric aerosols, in Global Climatology and Radiation Characteristics, A. Deepak, Hampton, Va., USA, 1991.

Claquin, T., Schulz, M., and Balkanski, Y.: Modeling the mineralogy of atmospheric dust sources, J. Geophys. Res., 104, 22 243–22 256, 1999.

Claquin, T., Schulz, M., Balkanski, Y., and Boucher, O.: Uncertainties in modeling the radiative forcing of mineral dust, Tellus, 50B, 491–505, 1998.

Deer, W. A., Howie, R. A., and Zussman, J.: An introduction to the rock-forming minerals, New York, John Wiley and Sons, Inc., 528 p, 1966.

Dubovik, O., Holben, B., Eck, T., Smirnov, A., Kaufman, Y., King, M., Tanré, D., and Slutsker, I.: Variability of absorption and optical properties of key aerosol types observed in world-wide locations, J. Atmos. Sci., 59, 590–608, 2002.

Egan, W. G. and Hilgeman, T. W.: Optical Properties of Inhomogeneous Materials: Applications to Geology, Astronomy, Chemistry, and Engineering, Academic Press, 235 pp, 1979.

Giorgi, F. and Chameides, W. L.: Rainout lifetimes of highly soluble aerosols and gases as inferred from simulations with a general circulation model, J. Geophys. Res., 91, 14 367–14 376, 1986.

Fouquart, Y. and Bonnel, B.: Computations of solar heating of the Earth's atmosphere: A new parameterization, Beitr. Phys. Atmos., 53, 35–63, 1980.

Guelle, W., Balkanski, Y., Schulz, M., Marticorena, B., Bergametti, G., Moulin, C., Arimoto, R., and Perry, K. D.: Modelling the atmospheric distribution of mineral aerosol: Comparison with ground measurements and satellite observations for yearly and synoptic time scales over the North Atlantic, J. Geophys. Res., 105, 1997–2005, 2000.

Guelle, W., Schulz, M., Balkanski, Y., and Dentener, F.: Influence of the source formulation on modeling the atmospheric global distribution of sea-salt aerosol, J. Geophys. Res., 106, 27 509–27 524, 2001.

Hauglustaine, D. A., Hourdin, F., Jourdain, L., Filiberti, M.-A., Walters, S., and Lamarque, J.-F.: Interactive chemistry in the Laboratoire de Météorologie Dynamique general circulation model: description and background tropospheric chemistry evaluation, J. Geophys. Res., 109, D04314, doi:10.1029/2003JD003957, 2004.

Haywood, J. M., Francis, P., Osborne, S., et al.: Radiative properties and direct radiative effect of Saharan dust measured by the C-130 aircraft during Saharan Dust Experiment (SHADE). 1: Solar spectrum, J. Geophys. Res., 108(D18), doi:10.1029/2002JD002687, 2003.

Hourdin, F., Musat, I., Bony, S., Braconnot, P., Codron, F., Dufresne, J.-L., Fairhead, L., Filiberti, M.-A., Friedlingstein, P., Grandpeix, J.-Y., Krinner, G., LeVan, P., Li, Z.-X., and Lott, F.: The LMDZ general circulation model: climate performance and sensitivity to parameterized physics with emphasis on tropical convection, Clim. Dynamics, 1–27, doi:10.1007/s00382-006-0158-0, 2006.

Hunt, J. M., Wisherd, M. P., and Bonham, L. C.: Infrared absorption spectra of minerals and other inorganic compounds, Anal. Chem., 22, 1478–1497, 1950.

Kaufman, Y. J., Tanré, D., Dubovik, D. O., Karnieli, A., and Remer, L. A.: Absorption of sunlight by dust as inferred from satellite and ground-based remote sensing, Geophys. Res. Lett., 28,

1479–1482, 2001.
Liao, H. and Seinfeld, J. H.: Radiative forcing by mineral dust aerosols: sensitivity to key variables, J. Geophys. Res., 103(D24), 31 637–31 646, doi:10.1029/1998JD200036, 1998.
Li, F., Vogelmann, A. M., and Ramanathan, V.: Dust aerosol radiative forcing measured from space over the Western Africa, J. Clim., 17(13), 2558–2571, 2004.
Liu, H., Jacob, D. J., Bey, I., and Yantosca, R. M.: Contraints from 210Pb and 7Be on wet deposition and transport in a global three-dimensional chemical transport model driven by assimilated meteorological fields, J. Geophys. Res., 106, 12 109–12 128, 2001.
Long, L. L., Querry, M. R., Beli, R. J., and Aiexander, R. W.: Optical properties of calcite and gypsum in crystalline and powdered form in the infrared and the far infrared, Infrar. Phys., 34, 191–201, 1993.
Mari, C., Jacob, D. J., and Bechtold, P.: Transport and scavenging of soluble gases in a deep convective cloud, J. Geophys. Res., 105, 22 255–22 268, 2000.
Mishchenko, M. I., Travis, L. D., Kahn, R. A., and West, R. A.: Modeling phase functions for dustlike tropospheric aerosols using a shape mixture of randomly oriented polydisperse spheroids, J. Geophys. Res., 102, 16 831–16 847, 1997.
Morcrette, J.-J.: Radiation and cloud radiative properties in the European Centre for Medium-Range Weather Forecasts forecasting systems, J. Geophys. Res., 96, 9121–9132, 1991.
Morcrette, J.-J. and Fouquart, Y.: The overlapping of cloud layers in shortwave radiation parameterizations, J. Atmos. Sci., 43, 321–328, 1986.
Moulin, C., Gordon, H. R., Banzon, V. F., and Evans, R. H.: Assessment of Saharan dust absorption in the visible from SeaWiFS imagery, J. Geophys. Res., 106(D16), 18 239–18 250, doi:10.1029/2000JD900812, 2001.
Myhre, G. and Stordal, F.: Global sensitivity experiments of the radiative forcing due to mineral aerosols, J. Geophys. Res., 106(D16), 18 193–18 204, doi:10.1029/2000JD900536, 2001.
Patterson, E. M., Filette, D. A., and Stockton, B. H.: Complex index of refraction between 300 and 700 nm for Saharan aerosols, J. Geophys. Res., 82, 3153–3160, 1977.
Peterson, J. T. and Weinmar, J. A.: Optical properties of Quartz dust particles at infrared wavelengths, J. Geophys. Res., 74, 6947–6952, 1969.
Popova, S. I., Tolstych, T. S., and Ivlevn, L. S.: Optical constants of Fe_2O_3 in the infrared spectral region, Optika Spektrosc., 35, 954–955,1973.
Querry, M., Osborne, P., Lies, K., Gordon, R., and Coveney, R. M.: Complex refractive index of limestone in the visible and infrared, Appl. Opt., 17, 353–356, 1978.

Roush, T., Pollack, J., and Orenberg, J.: Derivation of midinfrared (5–25 μm) optical constants of some silicates and palagonite, Icarus, 94, 191–208, 1991.

Schulz, M., Balkanski, Y., Dulac, F., and Guelle, W.: Treatment of aerosol size distribution in a global transport model: Validation with satellite-derived observations for a Saharan dust episode, J. Geophys. Res., 103, 10 589–10 592, 1998.

Shettle, P. E. and Fenn, R. W.: Models for the aerosols of the lower atmosphere and the effects of humidity variations on their optical properties, AFCRL Tech. Report, 79 0214, Research Papers No. 676, Air Force Cambridge Research Laboratory, Hanscom Airforce Base, MA., 100 pp, 1979.

Sokolik, I. N., Andronova, A. V., and Jonhson, T. C.: Complex refractive index of atmospheric dust aerosols, Atmos. Envir., 16, 2495–2502, 1993.

Sokolik, I. N. and Toon, O. B.: Direct radiative forcing by anthropogenic airborne mineral aerosols, Nature, 381, 681–683, 1996.

Sokolik, I. N. and Toon, O. B.: Incorporation of mineralogical composition into models of the radiative properties of mineral aerosol from UV to IR wavelengths, J. Geophys. Res., 104(D8), 9423–9444, doi:10.1029/1998JD200048, 1999.

Steyer, T. R., Day, L., and Huffman, D. R.: Infrared absorption by small amorphous quartz spheres, Appl. Opt., 13, 1586–1590, 1974.

Toon, O. B., Pollack, J. B., and Sagan, C.: Physical properties of the particles composing the martian dust storm of 1971–1972, Icarus, 30, 663–696, 1977.

Tegen, I. and Lacis, A. A.: Modeling of particle size distribution and its influence on the radiative properties of mineral dust aerosol, J. Geophys. Res., 101, 19 237–19 244, 1996.

Volz, F. E.: Infrared optical constants of ammonium sulphate, Saharan dust, volcanic pumice, and flyash, Appl. Opt., 12, 564–568, 1973.

Woodward, S.: Modeling the atmospheric life cycle and radiative impact of mineral dust in the Hadley Centre climate model, J. Geophys. Res., 106(D16), 18 155–18 166, doi:10.1029/2000JD900795, 2001.

Table 1. Refractive indices of the different minerals constitutive of dust and references used.

	Infrared spectrum
Quartz	Peterson and Weinmar (1969), Steyer et al. (1974), Hunt et al. (1950) (*)
Illite	Querry (1987), Hunt et al. (1950) (*)
Montmorillonite	Querry (1987), Toon et al. (1977), Hunt et al. (1950) (*)
Kaolinite	Roush et al. (1991), Hunt et al. (1950) (*)
Calcite	Querry et al. (1978), Long et al. (1993)
Hematite	Popova et al. (1973), Hunt et al. (1950) (*)
Goethite	Hunt et al. (1950) (*)
	Visible spectrum
Quartz	Peterson and Weinmar (1969), Deer (1966) ($^+$)
Montmorillonite	Egan and Hilgeman (1979), Lindberg and Suyder (1972)
Illite	Egan and Hilgeman (1979), Lindberg and Snyder (1972)
Kaolinite	Egan and Hilgeman (1979), Lindberg and Smith (1974)
Calcite	Deer et al. (1966) ($^+$)
Hematite	Bedidi and Cervelle (1993)
Goethite	Bedidi and Cervelle (1993)

* indicates data that had to be extrapolated
$^+$ indicates that a mean value was taken over the spectral interval considered

Table 2. Percentage of the volume for the 6 different minerals used to compute the refractive index, density for each of the minerals is, respectively, 5.3, 2.71, 2.65, 2.71 and 2.71 g cm^{-3}, for hematite, illite, quartz, calcite, kaolinite and montmorillonite.

	S1a Central Hematite	S1b High Hematite	S1c Low Hematite
Hematite	1.5	2.7	0.9
Illlite	31.5	30.3	32.1
Quartz	14.0	14.0	14.0
Calcite	6.0	6.0	6.0
Kaolinite	24.0	24.0	24.0
Montmorillonite	23.0	23.0	23.0
Total	100.0	100.0	100.0

Table 3. Annual mean Mineral Dust Forcing (SW+LW) over different regions.

Region	Case S1 (W m^{-2})	Case S2 (W m^{-2})
Tropical Atlantic	TOA=–6.1	TOA=–2.1
(14° N–24° N; 45° W–15° W)	SRF=–9.0	SRF=–12.4
	Heating*=–6.1–(–9.0)=+2.9	Heating=+10.3
Sahara	TOA=+2.0	TOA=+9.3
(14° N–29° N; 10° W–32° E)	SRF=–2.3	SRF=–6.4
	Heating=+4.3	Heating=+15.7
Sahel	TOA=–1.6	TOA=+2.2
(6° N–14° N; 10° W–32° E)	SRF=–3.7	SRF=–6.4
	Heating=+2.1	Heating=+8.6
Arabian Peninsula	TOA=–0.7	TOA=+3.4
(14° N–31° N; 32° E–58° E)	SRF=–3.6	SRF=–6.3
	Heating=+2.9	Heating=+9.7
Northern Indian Ocean	TOA=–2.9	TOA=–0.9
(1° N–21° N; 55° E–73° E)	SRF=–4.4	SRF=–6.2
	Heating=+1.5	Heating=+5.3
Asia	TOA=–1.6	TOA=+1.3
(24° N–51° N; 69° E–141° E)	SRF=–4.0	SRF=–6.1
	Heating=+2.4	Heating=+4.8

* The column heating (W m^{-2}) is computed as the difference between TOA and surface fluxes.

Table 4. Top of atmosphere (TOA) and surface (SRF) dust radiative effect (W m^{-2}).

Case	Load (mg m^{-2}) 0<D<1 μm	Load 1<D<10 μm	Total OD	SW TOA	LW TOA	SW+LW TOA	SW+LW SRF
1.5% hematite internally mixes							
S1 simulation (this study)	4.0	36.2	0.031	–0.68	+0.29	–0.39	–0.92
Refractive index Patterson-Volz							
S2 simulation (this study)	4.0	36.2	0.031	+0.05	+0.30	+0.35	–1.44
Tegen et al. (1996)	14.7	21.6	0.026	–0.39	+0.53	+0.14	–1.92
*Refractive index from a range of measurements**							
Woodward (2001)	NA	NA	NA	–0.16	+0.23	+0.07	–0.82
Refractive index from d'Almeida (1991)							
Myhre and Stordal (2001)	14.7	21.6	0.026	–0.61	+0.13	–0.48	NA
Same dust distribution as Tegen et al. (1996), same size distribution as Tegen and Lacis (1996)							

* references for these measurements: Carlson and Benjamin (1980), Sokolik et al. (1993, 1998), WMO (1993)

Table 5. Sensitivity study to MMD, mineral dust radiative forcing (W m^{-2}) at Top of the Atmosphere and at the surface.

Case	SW	LW	SW+LW TOA	SW+LW SRF
Internal mixtures (this study)				
S1: 1.5% hematite	–0.68	+0.29	–0.39	–0.92
S1b: 0.9% hematite	–0.76	+0.29	–0.47	–0.81
S1c: 2.7% hematite	–0.53	+0.29	–0.24	–1.11
External mixtures (this study)				
S3: 1.5% hematite	–0.38	+0.32	–0.06	–1.01
S3b: 0.9% hematite	–0.53	+0.32	–0.21	–0.80
S3c: 2.7% hematite	–0.15	+0.32	+0.17	–1.33
External mixtures (Myrhe and Stordal, 2001)				
0.5% hematite	–1.14	+0.42	–0.72	NA
1.0% hematite	–1.08	+0.41	–0.66	NA
Sensitivity study with 2 modes (this study) 1st mode with MMD=2.5 μm for and 2nd mode MMD=5.0 μm at the source				
S4: 1.5% hematite	–0.78	+0.38	–0.40	–1.13

Table 6. Clear-Sky Mineral Dust Radiative Efficiency ($Wm^{-2}\ \tau^{-1}$) Broadband Shortwave only. All values are averaged diurnally.

	TOA	Surface	Ratio [SRF/TOA]	Heating*
Summer (JJA) over the Tropical Atlantic (15° N–25° N; 45° W–15° W)				
Li et al. (2004)	–35±3	–65±3	1.9	+30±4
S1b: 0.9% Hematite	–49	–65	1.3	+16
S1: 1.5% Hematite	–47	–69	1.5	+22
S1c: 2.7% Hematite	–45	–76	1.7	+32
S2: Patterson-Volz	–29	–88	3.0	+60
30 Sept. 2000 near Dakar (15N,17W) values reported in Anderson et al. (2005) The model gridbox averages over (16.85° W–13.1° W and 13.75° N–16.25° N)				
Haywood et al. (2003)	–24	–38	1.6	+12
S1b: 0.9% Hematite	–24	–48	2.0	+24
S1: 1.5% Hematite	–21	–51	2.4	+30
S1c: 2.7% Hematite	–16	–57	3.6	+41
S2: Patterson-Volz	+4	–70	–17.5	+74

* The column heating ($W\ m^{-2}$) is computed as the difference between TOA and surface fluxes.

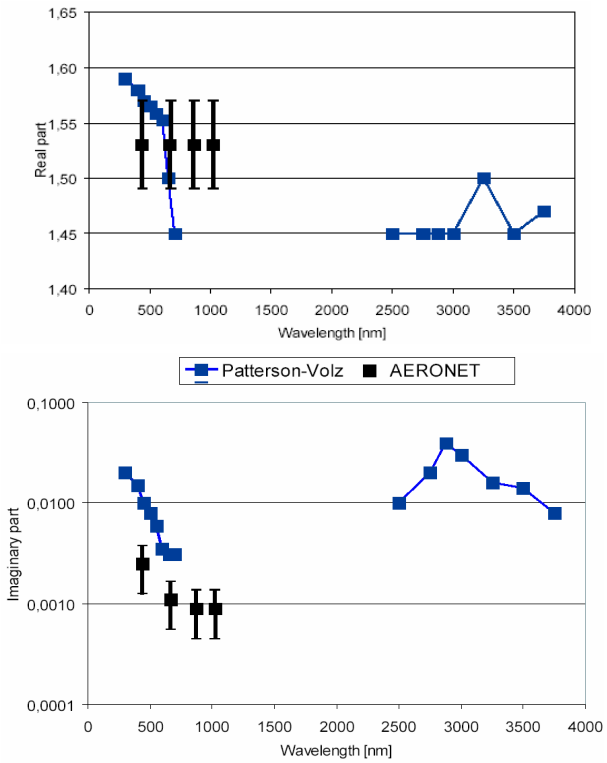

Fig. 1. Real and imaginary parts of mineral aerosol refractive indices. The filled blue squares indicate measurements that were collected by Patterson et al. (1977) between 300 and 700 nm and by Volz (1973) for wavelengths greater than 2500 nm. The AERONET measurements shown by the black squares are the ones reported by Dubovik et al. (2002). Uncertainties are ±0.04 on the real part of the refractive index and 50% on the imaginary part (Dubovik, 2002, and personal communication). The case that we refer to as *S2* or Patterson-Volz consists of a linear interpolation between the wavelengths 700 and 2500 nm.

ACPD
6, 8383–8419, 2006

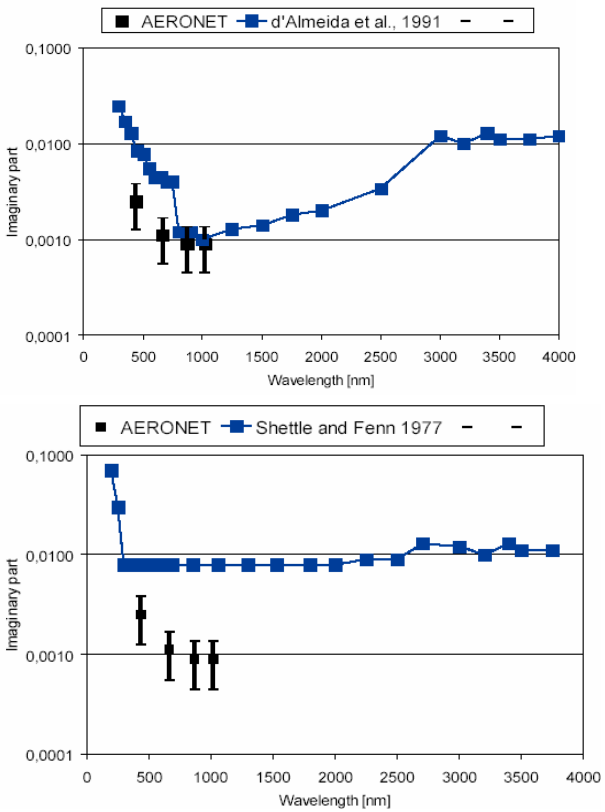

Fig. 2. Imaginary part of mineral aerosol refractive indices. The filled blue squares indicate measurements that were collected by d'Almeida et al. (1991) (top panel) and by Shetlle and Fenn (1979) (bottom panel). The filled black squares indicate the AERONET measurements reported by Dubovik et al. (2002). Uncertainties are as described for Fig. 1.

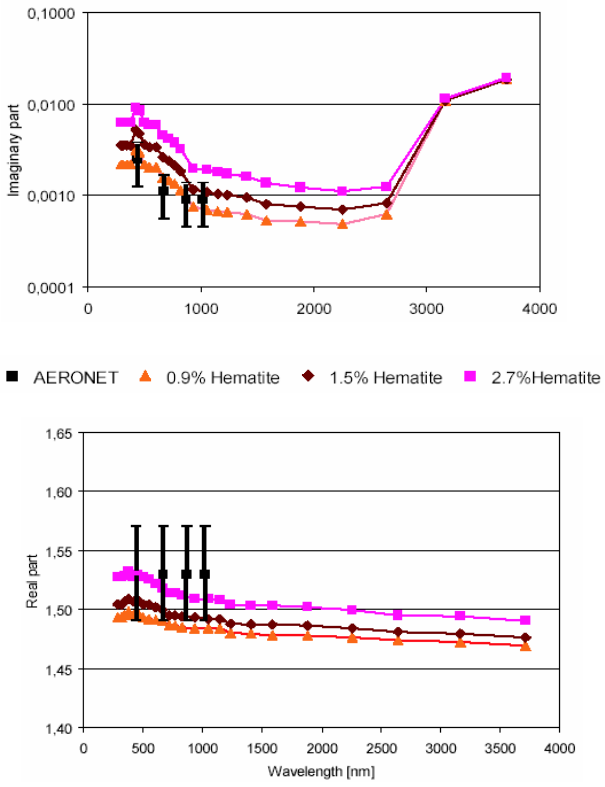

Fig. 3. Real and imaginary parts of mineral aerosol refractive indices. The solid triangles and squares are for an internal mixture with respectively 0.9, 1.5 and 2.7% hematite by volume. The AERONET measurements are the ones reported by Dubovik (2002). Uncertainties are 0.04 on the real part of the refractive index and 50% on the imaginary part (Dubovik, 2002, and personal communication).

ACPD
6, 8383–8419, 2006

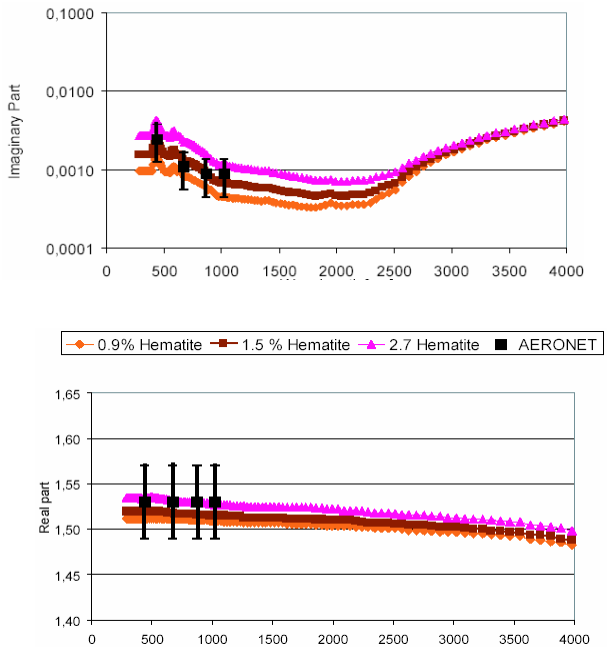

Fig. 4. Real and imaginary parts of mineral aerosol refractive indices. The solid triangles and squares are for an internal mixture with respectively 0.9%, 1.5 and 2.7% hematite by volume. The hematite is present as a coating over the other 5 other minerals (calcite, quartz, illite, kaolinite and montmorillonite). The refractive index of the internal mixture is computed using the Maxwell Garnett approximation given in Eq. (1) (see text). The AERONET measurements are the ones reported by Dubovik (2002). Uncertainties are 0.04 on the real part of the refractive index and 50% on the imaginary part (Dubovik, 2002, and personal communication).

ACPD
6, 8383–8419, 2006

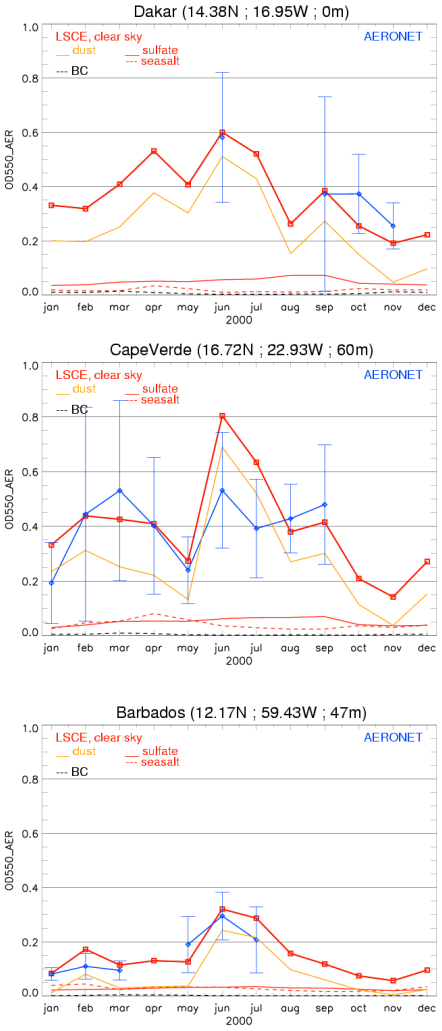

Fig. 5. Comparison of simulated optical depth at 550 nm to AERONET retrieved ones for 3 stations over Africa and across the tropical Atlantic in blue. The solid lines are yellow for dust and red for sulphate. The dashed lines represent the simulated OD for black carbon. There are black for carbon and red for seasalt.

ACPD
6, 8383–8419, 2006

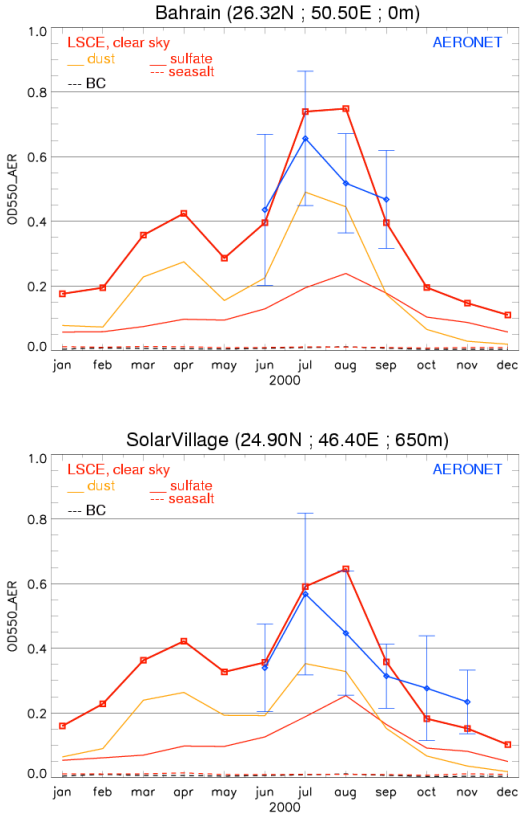

Fig. 6. Comparison of simulated optical depth at 550 nm to AERONET retrieved ones for 2 stations on the Arabian Peninsula in blue. The solid lines are yellow for dust and red for sulphate. The dashed lines represent the simulated OD for black carbon. There are black for carbon and red for seasalt.

ACPD
6, 8383–8419, 2006

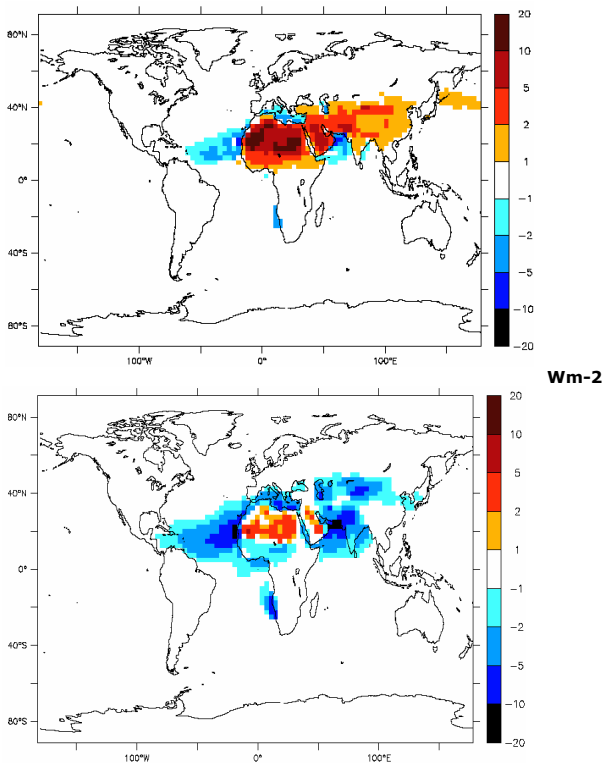

Fig. 7. Comparison of TOA radiative forcing of dust for 2 different hypotheses for dust refractive index: Top panel: Patterson and Volz; Bottom Panel: 1.5% by volume hematite content internally mixed.

ACPD
6, 8383–8419, 2006

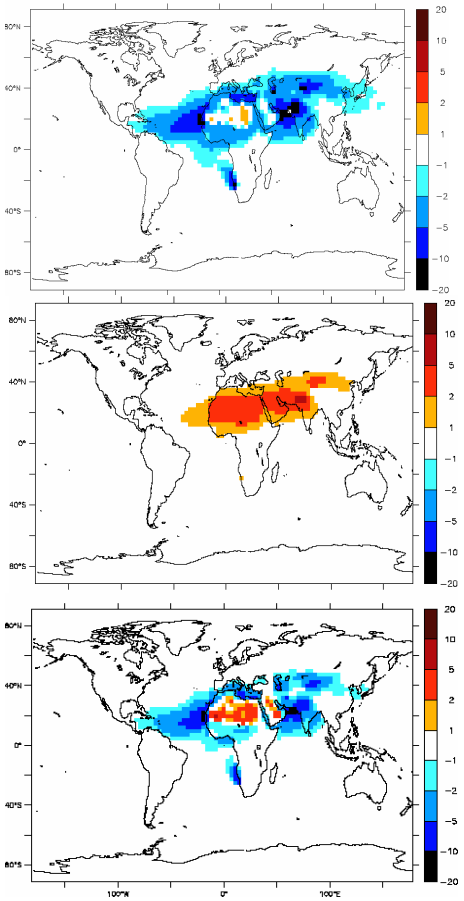

Fig. 8. TOA radiative forcing (Wm^{-2}) of mineral dust, the hematite represents 1.5% (by volume) of the minerals and the minerals are internally mixed. The Top, middle and bottom panels represent respectively the SW, LW, and the sum of SW+LW.

ACPD
6, 8383–8419, 2006

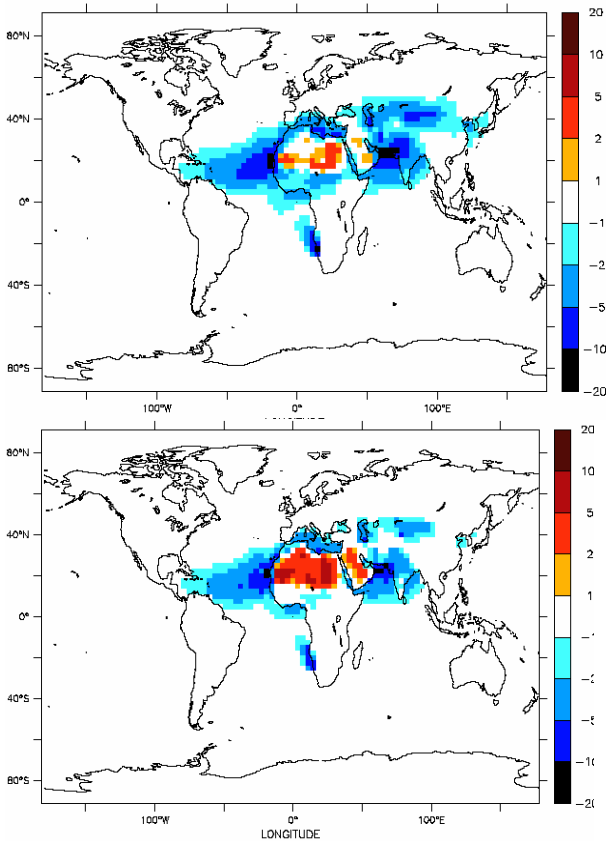

Fig. 9. TOA radiative forcing (Wm^{-2})from mineral dust (SW+LW), the hematite is internally mixed and the top and bottom panels are for respectively 0.9 and 2.7% hematite (volume content).

ACPD
6, 8383–8419, 2006